Journal of Alloys and Compounds 630 (2015) 48–53

Contents lists available at ScienceDirect

Journal of Alloys and Compounds

journal homepage: www.elsevier.com/locate/jalcom

$BiFeO_3$ tailored low loss M-type hexaferrite composites having equivalent permeability and permittivity for very high frequency applications

Yun Peng [a], Xiaohan Wu [a], Zhongyan Chen [a,c], Weihu Liu [a], Fan Wang [a], Xian Wang [a], Zekun Feng [a,*], Yajie Chen [b], Vincent G. Harris [b]

[a] School of Optical and Electronic Information, Huazhong University of Science and Technology, Wuhan 430074, China
[b] Center for Microwave Magnetic Materials and Integrated Circuits, and Department of Electrical and Computer Engineering, Northeastern University, Boston, MA 02115, USA
[c] Jiangmen Magsource New Material Co., Ltd, 529000 Guangdong, China

ARTICLE INFO

Article history:
Received 1 December 2014
Received in revised form 6 January 2015
Accepted 7 January 2015
Available online 13 January 2015

Keywords:
M-type hexaferrite
Low loss
Solid-state reaction method

ABSTRACT

Co–Ti substituted M-type hexaferrite composites, consisting of $Ba(CoTi)_{1.2}Fe_{9.6}O_{19}$ with various amounts of Bi_2O_3 (0–8 wt%), were successfully synthesized by conventional ceramic processes. The effects of Bi_2O_3 upon the composite microstructure, magnetic properties, and magnetic and dielectric properties sintered at low temperatures were systematically investigated. The present studies aim to develop magneto-dielectric materials possessing equivalent values of permeability and permittivity, as well as low magnetic and dielectric losses, which allow for miniaturizing efficient antennas at the very high frequency band (VHF, 30–300 MHz). The present experiments show that addition of $BiFeO_3$, observed in the polycrystalline hexaferrite composites, acts to reduce loss factors (i.e., $\tan \delta_\mu/\mu' = 0.014$, $\tan \delta_\varepsilon/\varepsilon' = 0.00071$) while concomitantly retaining high and equivalent values of permeability and permittivity (i.e., $\mu' \sim 12$ and $\varepsilon' \sim 12$ at 300 MHz).

1. Introduction

In recent decades, the rise of mobile systems and devices for personal data communications and multimedia digital broadcasting services, the communication technologies, materials, and devices operating at very high frequency (VHF) (i.e., 30–300 MHz) have attracted much attention. Among those applications, radio frequency (rf) antenna are assuredly one of the most important components in VHF systems. However, the length of antenna is usually required to be a quarter of the electromagnetic wave in vacuum, e.g., ~40 cm for VHF applications [1]. This is obviously too large to be used for mobile devices or in compact systems. Some solutions to reducing the size of antennas are proposed. (a) The design of miniature antenna structures may result in poor figures of merit (FOM). (b) Use of high dielectric constant materials leads to the drawbacks [2–4]. The electromagnetic field is confined to an area with high permittivity, yielding poor efficiency and narrow bandwidth of the antenna). In addition, due to low characteristic impedance, it is difficult for the high dielectric constant material to impedance match the antenna. Finally, (c) these issues could be overcome by using the magneto-dielectric materials having high and equivalent values of permeability and permittivity. A transmission wavelength inside an antenna base can be calculated in terms of the formula $\lambda = c/f\sqrt{\varepsilon_r\mu_r} \approx c/f\sqrt{\varepsilon'\mu'}$ (λ is the transmission wavelength, c is the velocity of light, f is the transmission frequency, ε_r is the relative permittivity, μ_r is the relative permeability, ε' is the real permittivity and μ' is the real permeability.), where the dielectric loss and magnetic loss are assumed to be very small. It is no doubt that increasing permeability is superior to increasing permittivity to reduce the size of the antenna [5]. Additionally, the impedance of antenna is calculated in terms of the following formula, $Z = \sqrt{\mu_0\mu_r/\varepsilon_0\varepsilon_r} \approx \sqrt{\mu_0\mu'/\varepsilon_0\varepsilon'} = \eta_0$ (where Z is the impedance of the antenna, μ_0 is the permeability of free space, ε_0 is the permittivity of free space and η_0 is the impedance of free space). It is clear that the impedance of the materials used for antenna is the same as free space for the case in which magnetic permeability (μ') and permittivity (ε') are equivalent [6–8]. Furthermore, it is clearly important for the design of high efficiency antennas when both dielectric and magnetic loss of the magnetic materials are low, i.e. low loss tangent values. However, it is extremely challenging to achieve the desired materials having relatively high permeability, low permittivity and equivalent μ' and ε' at certain frequency

* Corresponding author.
E-mail address: fengzekun@hust.edu.cn (Z. Feng).

http://dx.doi.org/10.1016/j.jallcom.2015.01.026
0925-8388/

bands. This is a primary goal of the rf magnetics community and communication industry.

Generally, ferrite materials not only have low permittivity and high magnetic permeability, but also possess high electrical resistivity. There is no doubt that ferrites are ideal materials for use in miniature high frequency antennas. In the ferrite family, either spinel or hexagonal ferrites are often used for the design of antennas, depending upon the operating frequency of antennas. Spinel ferrites have high permeability, but the cutoff frequency is low (~300 MHz) due to Snoek's limit [9]. Accordingly, the operating frequency of spinel ferrites is usually below 100 MHz, whereas hexagonal ferrites, with high magneto-crystalline anisotropy and cutoff frequencies >1 GHz, can operate at a high frequency (VHF). Hexagonal ferrites show permeability much lower than that of spinel ferrites at low frequencies, but they are irreplaceable at high frequencies (>100 MHz).

Eventually, ferrite antenna materials have been widely investigated in order to gain low losses and equivalent values of permeability and permittivity [10,11]. Either spinel or hexagonal ferrites may be effective candidates as antenna substrate materials depending upon the selection of operating frequencies. Therefore, the Co_2Z hexagonal ferrite has been investigated for many years due to its easy *c*-plane and high permeability that are available for microwave devices [12–15]. Previous studies on Co_2Z ferrites demonstrated equivalent values of μ' and ε' (i.e., ~13), however magnetic loss tangents were >0.05 and >0.1 at a frequency beyond 100 MHz and 250 MHz, respectively [5]. Additionally, high sintering temperatures (>1200 °C) and complex phase transformation are often inevitable during optimal sintering processes for the Co_2Z ferrites, which indeed makes the formation of a single phase structure more difficult than other hexaferrites. Nevertheless, Su et al., have recently demonstrated in *Z*- and *Y*-phase mixed hexaferrites give rise to low magnetic and dielectric losses over a frequency range of $0.3 < f < 1$ GHz [16].

Among the hexaferrites, M-type hexagonal ferrite (BaM: $BaFe_{12}O_{19}$) is relatively simple in structure and fabrication processes. Therefore, here we propose three strategies to realize low temperature sintering, high permeability and low losses of the BaM ferrite: (1) an additive, such as Bi_2O_3, is employed to lower sintering temperatures and modify morphology of polycrystalline ferrites, while retaining the desired crystallographic structure and parameters; (2) low magnetic loss may be achieved by an extra phase e.g. $BiFeO_3$ having high electrical resistivity and weak magnetism; and, (3) the uniaxial (*c*-axis) magnetic anisotropy can be reduced and even transformed to the easy basal plane (*c*-plane) by the substitution of Fe in BaM ferrite with cations Sc^{3+}, ($Co^{2+} + Ti^{4+}$), etc. [17,26]. It is anticipated that such substitutions enable the enhancement of permeability due to the reduction in magnetic anisotropy energy. In present work, we investigate the microstructure, magnetic properties, and high frequency magnetic spectra of (CoTi)-doped BaM ferrite. Combined with a secondary phase of Bi_2O_3, the (CoTi)-doped BaM ferrites, are revealed to have low magnetic and dielectric losses, as well as high permeability at 10–300 MHz. Interestingly, equivalent values of permeability and permittivity were measured in the ferrite composites indicating characteristic impedance identical to that of free space.

2. Experimental procedure

$Ba(CoTi)_{1.2}Fe_{9.6}O_{19}$ M-type hexaferrites with various amounts of the secondary Bi_2O_3 phase (0–8 wt%) were prepared by solid-state reaction. Starting materials, reagent grade Fe_2O_3, $BaCO_3$, CoO, and TiO_2, were mixed for 1 h in a planetary ball-mill. The mixture was then calcined at 1100 °C for 2 h and ground with the Bi_2O_3 additive for an additional 2 h. The resultant powders were dry-pressed to form toroidal and disk-shaped samples, and finally sintered at 925 °C for 3 h in air.

The crystallographic structure and morphology of the samples were characterized by X-ray diffraction (XRD) and scanning electron microscope (SEM), respectively. Room temperature magnetic measurements were carried out using a vibrating sample magnetometer (VSM) with applied fields up to 15 kOe. The DC electrical resistivity of the obtained disk-shaped samples was measured with Ag electrodes via the two-probe technique. The complex permeability and permittivity were measured using an Agilent E4991A RF Impedance/Materials Analyzer from 1 MHz to 1 GHz with 16454A and 16453A test fixtures.

3. Results and discussion

3.1. Structural characteristics

The XRD patterns of $Ba(CoTi)_{1.2}Fe_{9.6}O_{19} + Bi_2O_3$ (x = 0–8 wt%) hexaferrite composites are illustrated in Fig. 1. It is found that the $Ba(CoTi)_{1.2}Fe_{9.6}O_{19}$ ferrites show a single phase structure until the Bi_2O_3 content exceeds 5 wt%. It is assumed that when small amounts of Bi_2O_3 are introduced, Bi^{3+} ions enter the lattice of the hexagonal phase. A second phase of $BiFeO_3$ was verified as the doping of Bi_2O_3 was increase beyond 5 wt%. It is well known that $BiFeO_3$ is a multiferroic material, presenting both ferroelectric and weak ferromagnetic response at room temperature [18]. It is predictable that the highly electrically resistive phase may reduce the magnetic loss of the ferrites. This assumption will be revealed and discussed in later sections.

3.2. Morphology of samples

Fig. 2(a) presents the morphology of $Ba(CoTi)_{1.2}Fe_{9.6}O_{19}$ ferrites with different Bi_2O_3 contents. It is noticed that the average grain size increases from 0.54 to 1.94 μm due to the Bi_2O_3-assisted sintering for low doping levels of Bi_2O_3. However, crystal growth may be inhibited with excessive Bi_2O_3, (i.e., great than 5 wt%), leading to a reduction of the average grain size to ~1.47 μm, as depicted in Fig. 2(b). We show that the introduction of bismuth oxide is able to lower sintering temperatures due to the low melting temperature (820 °C) of Bi_2O_3. Liquid-phase assisted solid phase sintering is more likely to give rise to large grains and high density in polycrystalline ferrites. It is therefore somewhat surprising that a high concentration of ($\geqslant$5 wt%) of Bi_2O_3 does not result in a visible increase in the grain size. Actually, a liquid phase layer not only accelerates the mass transfer but also generates a wetting meniscus at grain boundaries, providing an additional capillary pressure drive force during the high temperature sintering process [19]. It is speculated that the grain growth is restricted because of the thick liquid phase layer generated by excessive Bi_2O_3 ($\geqslant$5 wt%).

3.3. Static magnetic properties

Fig. 3(a) shows magnetic hysteresis loops of $Ba(CoTi)_{1.2}Fe_{9.6}O_{19}$ ferrites with various Bi_2O_3 contents. The values of magnetization

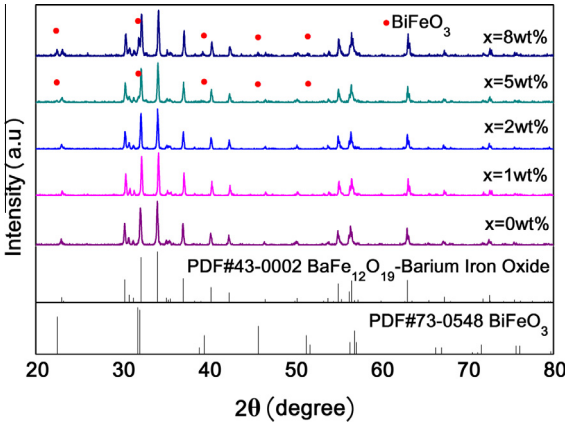

Fig. 1. XRD patterns of the samples sintered at 925 °C with different Bi_2O_3 contents (x wt%).

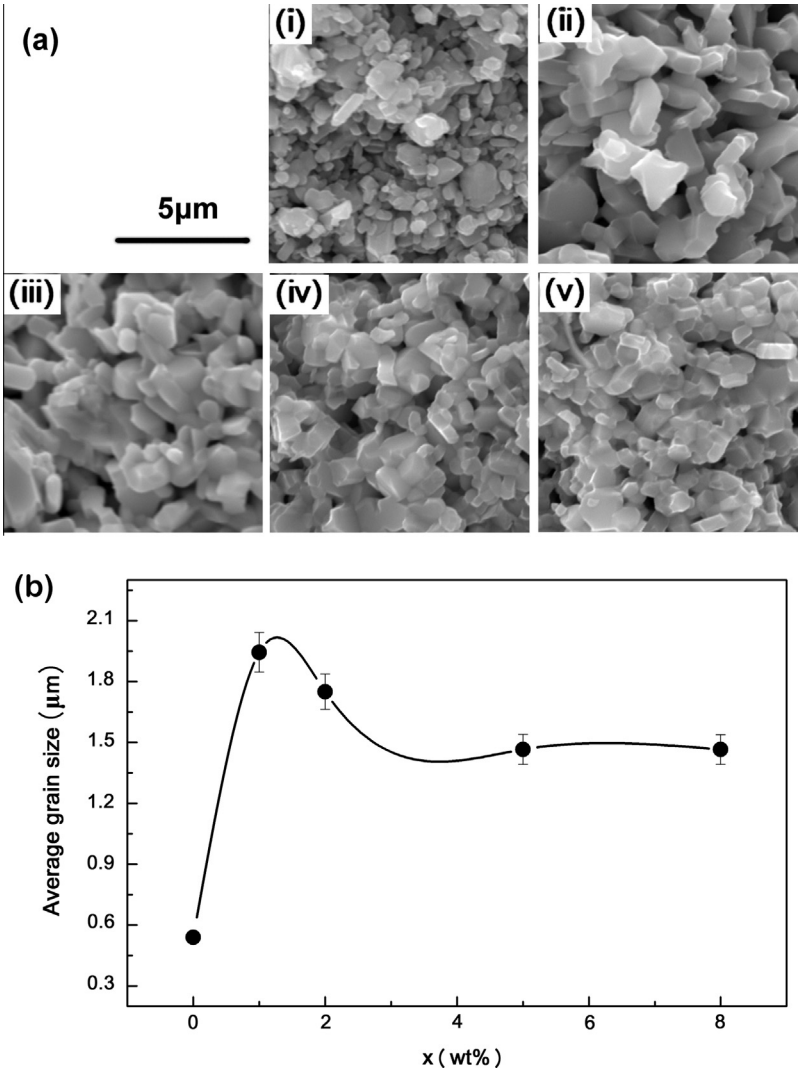

Fig. 2. (a) SEM images of the sample surfaces sintered at 925 °C with various Bi_2O_3 contents. (i) 0 wt%, (ii) 1 wt%, (iii) 2 wt%, (iv) 5 wt% and (v) 8 wt%. (b) Variation of average grain size D with Bi_2O_3 content.

(M_{15kOe}) at H = 15 kOe and coercivity (H_c) for all samples are illustrated in Fig. 3(b). The measured magnetization reveals a maximum at 2 wt% Bi_2O_3, i.e., M_{15kOe} increases from 231 G to 244 G with Bi_2O_3 $x < 2$ wt%, whereas it decreases as x exceeds beyond 2 wt%. The increase in magnetization may arise from the substitution of Bi^{3+} for Fe [20]. An excessive Bi^{3+} results in the appearance of the secondary phase, leading to a reduction in magnetization. It is worth noting that the coercivity shows an opposite trend to magnetization with Bi_2O_3 x content, which is attributed to magnetocrystalline anisotropy field and grain size. Firstly, a magentocrystalline anisotropy field is expressed as $H_k = 2K_{u1}/M_s$ (H_k is the magentocrystalline anisotropy field, K_{u1} is the first-order anisotropy constant and M_s is the saturation magnetization). It implies that a ratio of K_{u1} to M_s determines anisotropy field and ultimately affects coercivity. Secondly, coercivity is associated with particle size or grain size in a polycrystalline ferrite, closely depending upon the single domain size [21]. If a grain forms multiple domains, coercivity becomes inversely proportional to the grain size. In the present work, the observation in coercivity is assumed to arise predominately from magnetization and grain size with Bi doping. This will be verified with more measurements and calculations presented in the next section.

To obtain the first-order anisotropy constant for the samples studied, the law of approach to saturation (LAS) is employed to determine more accurately the saturation magnetization and anisotropy constant. It is well-known for a polycrystalline sample that a magnetization follows with a LAS, supposing that a magnetization is only attributed to the spin-rotation process at relatively high fields, as described below [22],

$$M = M_s\left(1 - \frac{A}{H} - \frac{B}{H^2}\right) + \chi H \tag{1}$$

where χH and M_s stands for the field-induced forced magnetization term, and the spontaneous saturation magnetization of domains, respectively. A is a constant associated with the effects of inclusions and micro-stress while B is related to the contribution of magnetocrystalline anisotropy. For hexagonal crystals, the magnetocrystalline anisotropy term is given by [23]:

$$B = 4K_{u1}^2/15M_s^2 \tag{2}$$

The plots of the magnetization vs. $1/H^2$ at high fields for each of the samples show straight line curves (Fig. 4) meaning that the contributions of the inclusions/micro-stresses and the magnetization terms are negligible. The saturation magnetization values for all of the samples are derived from the straight line extrapolation to $1/H^2 \rightarrow 0$. The first-order anisotropy constant K_{u1} is determined from the slope of the straight line in terms of Eq. (2). The results are

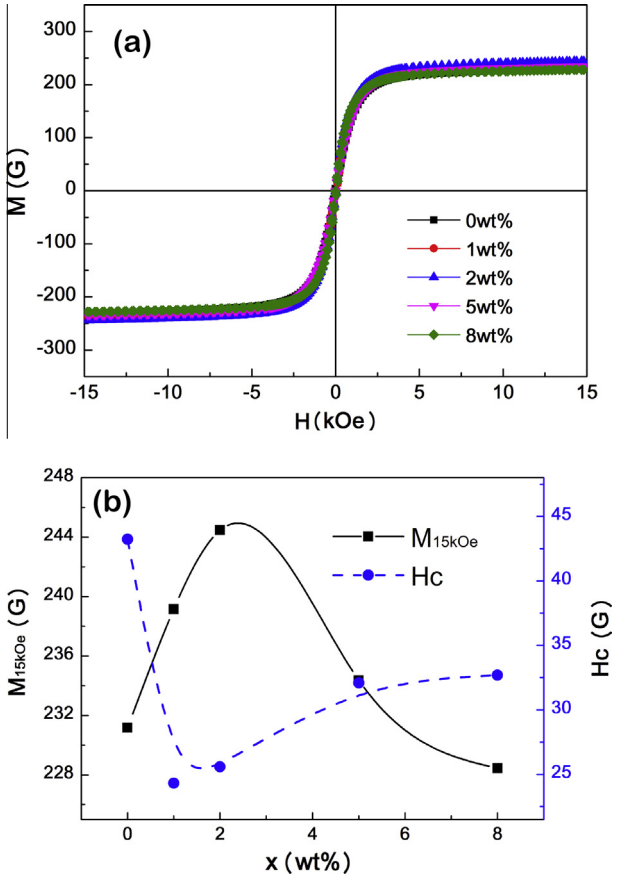

Fig. 3. (a) Magnetic hysteresis loops of $Ba(CoTi)_{1.2}Fe_{9.6}O_{19}$ with various Bi_2O_3 contents, and (b) variation of M_{15kOe} and H_c with various Bi_2O_3 contents.

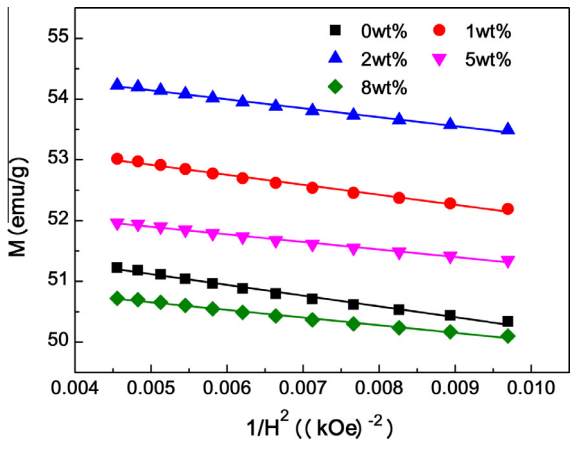

Fig. 4. High field magnetization vs. $1/H^2$ for $Ba(CoTi)_{1.2}Fe_{9.6}O_{19}$ ferrites with various Bi_2O_3 contents.

illustrated in Fig. 5, which clearly shows a decrease in K_{u1} with Bi_2O_3. M_s increases from 240 G to 252 G with Bi_2O_3 contents $x < 2$ wt%, whereas it decreases as x exceeds 2 wt%. The first-order anisotropy constant K_{u1} remains positive, though the doping of Bi ion reduces significantly K_{u1} from 3.923×10^5 erg/cm^3 to 3.277×10^5 erg/cm^3. This implies that the Bi-doped BaM retains perpendicular anisotropy, i.e., the c-axis remains the principle easy axis. In theory, it can be predicted that small anisotropy constants give rise to high permeability. This is a key supposition in the present studies to tailor the dynamic response of magnetic properties while retaining high permeability.

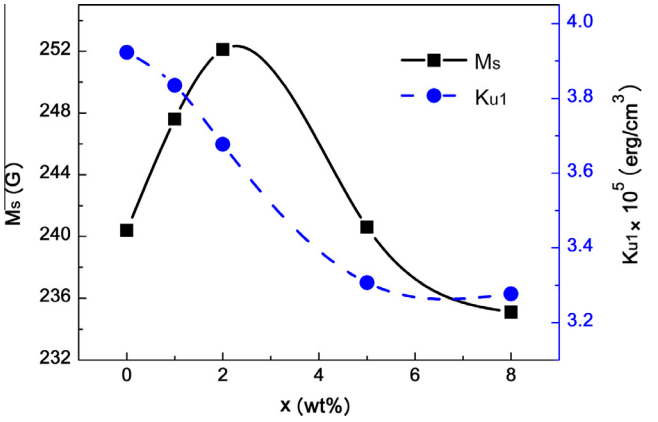

Fig. 5. Saturation magnetization M_s and first anisotropy constant K_{u1} of $Ba(CoTi)_{1.2}Fe_{9.6}O_{19}$ with various Bi_2O_3 contents.

According to the values presented in Fig. 5, a critical size of the single domain is estimated to be approximately 0.2 μm for all of the samples studied. This value derives from the equations, $\gamma = 4\sqrt{AK_{u1}}$ and $d = 2r_c = \frac{9\gamma\mu_0}{I_s^2} = \frac{9\gamma}{\mu_0 M_s^2}$ [24], where γ is the domain wall energy density, the exchange stiffness constant A is 4.1×10^{-7} erg/cm [25], and d is the critical size. The estimated size of the single domain provides direct evidence that the samples are of multiple domain structures. As such, the coercivity in the present materials should decrease with increasing grain size. This is clearly a result of the measurements presented in Fig. 3(b).

3.4. Complex permeability

The frequency dependence of complex permeability of the samples was measured over a frequency range of 1–1000 MHz, as depicted in Fig. 6. The real permeability (μ') remains almost constant with frequency until ~100 MHz. It is impressive that Bi_2O_3 not only enhances permeability, but also maximizes permeability as Bi_2O_3 is $x = 1$–2 wt%. Naturally, an increase in permeability results in reduction in the cut off frequency in terms of the Snoek's law [26]. It was measured that the cutoff frequency changes with permeability accordingly, as shown in Fig. 6(b).

In the ferrite materials, an initial permeability of crystal is predominantly determined by the saturation magnetization (M_s) and the first-order anisotropy (K_{u1}) constant as described below [27],

$$\mu \propto \frac{M_s^2}{K_{u1} + \lambda_s \sigma} \tag{3}$$

where λ_s and σ denote the magnetostriction coefficient and internal stress, respectively. The term $\lambda_s\sigma$ is often negligible because of very low stress in the ferrites. It is reasonable that the sample with 2 wt% of Bi_2O_3 exhibits the highest μ' at 1 MHz due to high M_s and low anisotropy constant, as shown in Fig. 5. Obviously, a high doping level of Bi_2O_3 leads to a decrease in both M_s and K_{u1}. However, it is deduced from the experimental data that the reduction in M_s is faster than that of K_{u1} with the introduction of Bi_2O_3. It ultimately reduces permeability, as shown in Fig. 6(a) and (b).

3.5. Complex permittivity

Fig. 7 depicts dielectric spectra for the samples with different Bi_2O_3 contents. We noticed that the real permittivity (ε') increases with the doping of Bi_2O_3 from 8 to 14, but it remains constant for all of the samples as frequency is lower than ~300 MHz. Over the operating frequency band of 50–300 MHz, the dielectric loss (ε'') changes slightly with Bi_2O_3 content.

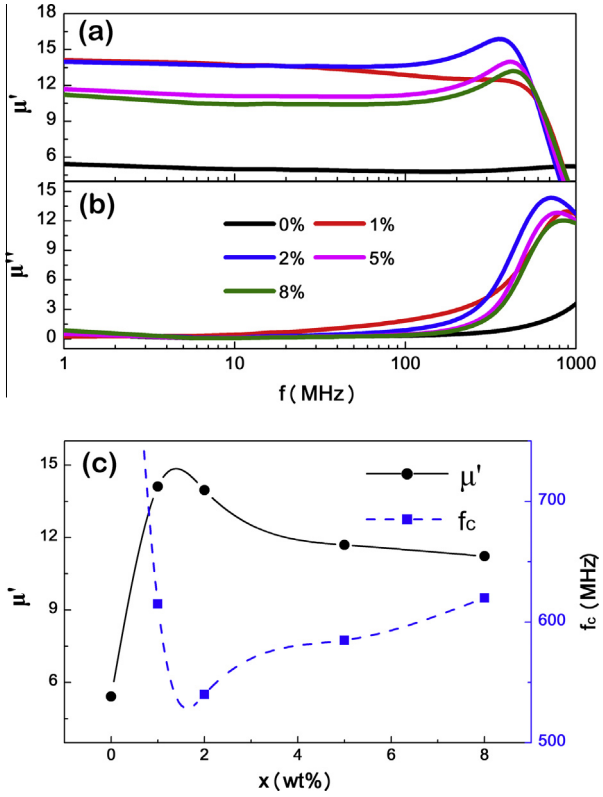

Fig. 6. (a and b) Complex permeability of $Ba(CoTi)_{1.2}Fe_{9.6}O_{19}$ with various Bi_2O_3 contents, and (c) the dependence of permeability μ' at 1 MHz and the cutoff frequency on Bi_2O_3 content.

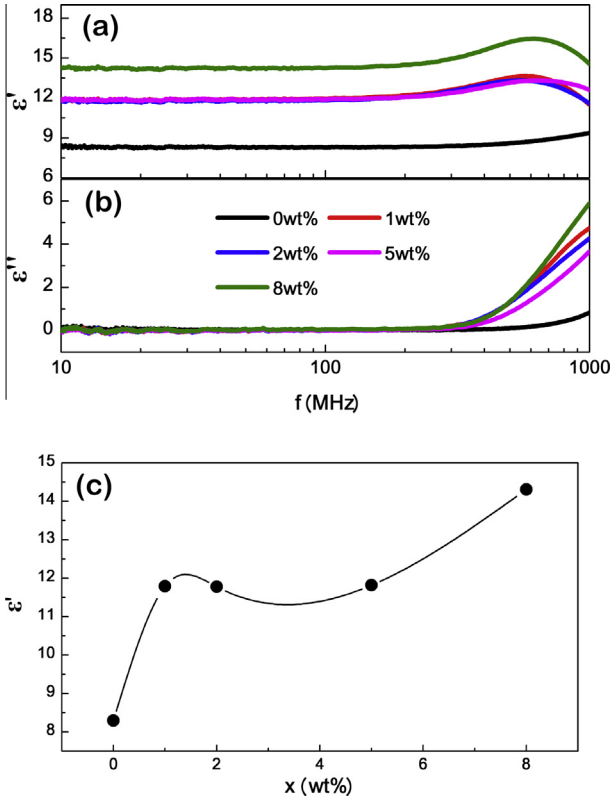

Fig. 7. (a and b) Complex permittivity of $Ba(CoTi)_{1.2}Fe_{9.6}O_{19}$ with various Bi_2O_3 contents, and (c) the dependence of permittivity ε' at 10 MHz on Bi_2O_3 content.

Real permeability and permittivity, magnetic and dielectric losses, as well as loss factors at 200 and 300 MHz are summarized in Table 1. It is found that permeability exhibits a maximum at $x = 2$ wt% Bi_2O_3, but magnetic loss tangent decreases linearly with Bi_2O_3. It is not surprising that low permeability corresponds to low loss tangent. To obtain figure of merit (FOM) of a material, loss factor ($\tan\delta/\mu'$) must be employed to evaluate a measure of effectiveness. Actually, a number of previous works have focused on ferrite materials used for antenna at operating frequencies (<200 MHz) [11]. Compared to the early reported data ($\mu' = 10.5$, $\tan\delta_\mu = 0.118$ at 200 MHz) [28], the present work reveals significant high permeability (~12) and low magnetic loss (~0.092) at 200 MHz. Furthermore, the BFO-tailored BaM ferrites present more promising data, i.e., both magnetic and dielectric loss factors are very low ($\tan\delta_\mu/\mu' = 0.014$, $\tan\delta_\varepsilon/\varepsilon' = 0.0007$) at 300 MHz. The super low loss factors may arise from the existence of the BFO phase in the BaM hexaferrite. It is believed that the multiferroic BFO phase effectively lowers magnetic loss at high frequency because of its high resistivity, as presented in Fig. 8. It is tangible that the resistivity increases slightly with Bi_2O_3 ($x \leqslant 2$ wt%), without any secondary phases detected. However, the existence of the BFO phase enhances markedly one order of magnitude of resistivity, corresponding to $x \geqslant 5$ wt%.

In addition to high resistivity, BFO may also contribute to the enhancement in magnetization of the polycrystalline ferrite owing to its weak ferromagnetism at room temperature [29]. Interestingly, BFO phase modifies magnetic and dielectric properties of the hexaferrites, especially favorable to reduce magnetic losses. High frequency permittivity of the ferrites mainly comes from the atomic, ionic and electronic polarization [30,31]. Moreover, material microstructure, grain size, porosity and impurities also have a great influence on dielectric properties of materials. It is considered that BFO not only affects microstructure (e.g., grain boundary), but also directly alters the effective permittivity of the polycrystalline ferrites. It is seen that the measured permittivity is increased because single phase BFO has a higher permittivity ($\varepsilon' \sim 40$) than that of the ferrites ($\varepsilon' \sim 20$) over the same frequency range [28]. However, the physical understanding of this phenomenon remains unclear. As a result, the best sample among those Bi_2O_3-doped BaM ferrites ($x = 5$ wt%) has demonstrated: $\mu' = 13.04$, $\tan\delta_\mu = 0.187$, $\varepsilon' = 12.37$, $\tan\delta_\varepsilon = 0.0087$, corresponding to loss factors, $\tan\delta_\mu/\mu = 0.0143$ and $\tan\delta_\varepsilon/\varepsilon = 0.0007$ at $f = 300$ MHz.

It is promising that the frequency dependence of permittivity or permeability for the sample with the secondary phase BFO ($x = 5$ wt%) is almost constant over the broad frequency range 10–300 MHz. Moreover, this sample exhibits equivalent values of μ' and ε', which means an ease in impedance matching, i.e., the characteristic impedance of the material is the same as the impedance of the free space. In the meanwhile, a miniaturization factor

Table 1
μ', $\tan\delta_\mu$, $\tan\delta_\mu/\mu'$, ε' and $\tan\delta_\varepsilon$ of $Ba(CoTi)_{1.2}Fe_{9.6}O_{19}$ with various Bi_2O_3 contents at 200 MHz and 300 MHz.

Bi_2O_3 (wt%)	f (MHz)	μ'	$\tan\delta_\mu$	$\tan\delta_\mu/\mu'$	ε'	$\tan\delta_\varepsilon$	$\tan\delta_\varepsilon/\varepsilon'$
0	200	4.785	0.09924	0.0207	8.39	0.00412	0.000491
1		12.53	0.2346	0.0187	12.20	0.00445	0.000365
2		14.46	0.137	0.00947	12.06	0.00375	0.000311
5		11.93	0.09178	0.00769	12.06	0.00299	0.000248
8		11.19	0.08031	0.00718	14.48	0.00557	0.000385
0	300	4.85	0.14018	0.0289	8.39	0.00412	0.000491
1		12.48	0.33645	0.0269	12.61	0.01649	0.001308
2		15.58	0.26754	0.01717	12.51	0.01475	0.001179
5		13.04	0.187	0.01434	12.37	0.00877	0.000709
8		12.19	0.1671	0.01371	14.93	0.01242	0.000832

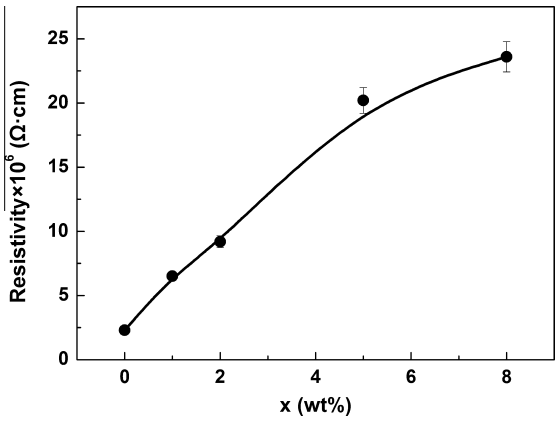

Fig. 8. Resistivity of $Ba(CoTi)_{1.2}Fe_{9.6}O_{19}$ with various Bi_2O_3 contents.

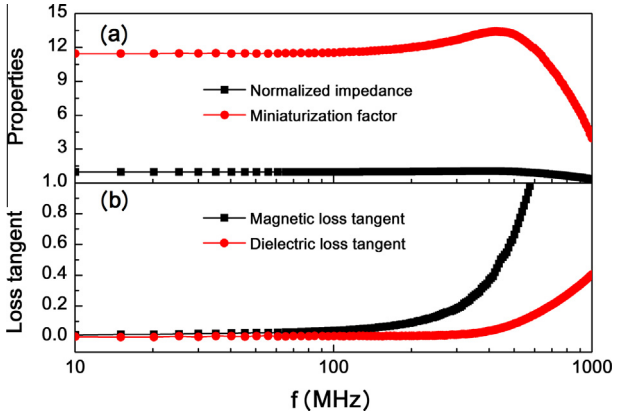

Fig. 9. Magneto-dielectric properties of $Ba(CoTi)_{1.2}Fe_{9.6}O_{19}$ with 5 wt% Bi_2O_3 sintered at 925 °C.

($n = \sqrt{\varepsilon_r \mu_r} \approx \sqrt{\varepsilon' \mu'}$) of ~12 and loss factors are estimated at the frequency range, as illustrated in Fig. 9(a) and (b). These data show high miniaturization factor and low loss factors compared to those reported data for random polycrystalline ferrites [28]. The present results hold great potential for use as substrates in efforts to miniaturize antenna operating at VHF frequencies.

4. Conclusion

Low loss and impedance matched $Ba(CoTi)_{1.2}Fe_{9.6}O_{19}$ M-type hexaferrites with various contents of Bi_2O_3 were investigated. The experiments indicate that Bi_2O_3 can significantly improve the sintering process at relatively low temperatures and modify morphology, crystallographic structure, and magnetic and dielectric properties of the hexaferrites. Interestingly, Bi_2O_3 enables the formation of a secondary phase, which was verified to be $BiFeO_3$ by XRD. The multiferroic BFO phase reduces both magnetic and dielectric losses, while sacrificing slightly permeability values: This may stem form high resistivity and the weak ferromagnetism of BFO. The BaM ferrites with BFO inclusions reveals equivalent μ' to ε', and very low loss factors, tan $\delta_\mu/\mu' \sim 0.01$, tan $\delta_\varepsilon/\varepsilon' < 0.0008$, at VHF frequencies of 10–300 MHz, while remaining a high miniaturization factor of ~12. These results have revealed potential to make antennas smaller, simpler in construction and at lower costs.

References

[1] S. Bae, Y.K. Hong, J.J. Lee, J. Jalli, G.S. Abo, W.M. Sung, G.H. Kim, S.H. Park, J.S. Kum, H.M. Kwon, IEEE Trans. Mag. 45 (2009) 4199.
[2] H. Mosallaei, K. Sarabandi, IEEE Trans. Antennas Propag. 52 (2004) 1558.
[3] Y.M. Tang, L. Jia, H.W. Zhang, B.Y. Liu, Microwave Opt. Technol. Lett. 54 (2012) 1380.
[4] K. Mohit, V.R. Gupta, N. Gupta, S.K. Rout, Ceram. Int. 40 (2014) 1575.
[5] H. Su, X. Tang, H. Zhang, Y. Jing, F. Bai, J. Electron. Mater. 43 (2014) 299.
[6] L.B. Kong, Z.W. Li, G.Q. Lin, Y.B. Gan, Acta Mater. 55 (2007) 6561.
[7] Y. Peng, B.M. Farid Rahman, X. Wang, G. Wang, J. Appl. Phys. 115 (2014) 17A505.
[8] J. Lee, Y.-K. Hong, W. Lee, J. Park, J. Mag. 18 (2013) 428.
[9] N.L. Andrey, N.R. Konstantin, J. Magn. Magn. Mater. 321 (2009) 2082.
[10] W. Zhang, Y. Bai, X. Han, L. Wang, X. Lu, L. Qiao, J. Cao, G. Dong, Mater. Res. Bull. 48 (2013) 3850.
[11] Q. Xia, H. Su, T. Zhang, J. Li, G. Shen, H. Zhang, X. Tang, J. Appl. Phys. 112 (2012) 043915.
[12] J. Lee, Y.-K. Hong, W.M. Seong, Microwave Opt. Technol. Lett. 53 (2011) 1222.
[13] Q. Xia, H. Su, T. Pan, T. Zhang, H. Zhang, X. Tang, J. Appl. Phys. 111 (2012) 063921.
[14] Y. Chen, A. Daigle, T. Fitchorov, B. Hu, M. Geiler, A. Geiler, C. Vittoria, V.G. Harris, Appl. Phys. Lett 98 (2011) 202502.
[15] V.G. Harris, IEEE Trans. Magn. Adv. Magn. 48 (2012) 1075.
[16] Z. Su, H. Chang, X. Wang, A.S. Sokolov, B. Hu, Y. Chen, V.G. Harris, Appl. Phys. Lett. 105 (2014) 062402.
[17] Y. Chen, M.J. Nedoroscik, A.L. Geiler, C. Vittoria, V.t.G. Harris, J. Am. Ceram. Soc. 91 (2008) 2952.
[18] T. Zhao, A. Scholl, F. Zavaliche, K. Lee, M. Barry, A. Doran, M.P. Cruz, Y.H. Chu, C. Ederer, N.A. Spaldin, R.R. Das, D.M. Kim, S.H. Baek, C.B. Eom, R. Ramesh, Nat. Mater. 5 (2006) 823.
[19] T. Zhou, H. Zhang, J. Jia, J. Li, Y. Liao, L.C. Jin, H. Su, J. Appl. Phys. 115 (2014) 17A511.
[20] A.G. Belous, O.I. V'yunov, E.V. Pashkova, V.P. Ivanitskii, O.N. Gavrilenko, J. Phys. Chem. B 110 (2006) 26477.
[21] G. Herzer, IEEE Trans. Magn. 26 (1990) 1397.
[22] B.D. Cullity, C.D. Graham, Introduction to Magnetic Materials, second ed., Wiley, Hoboken, New Jersey, 2009.
[23] M. Awawdeh, I. Bsoul, S.H. Mahmood, J. Alloys Comp. 585 (2014) 465.
[24] S. Chikazumi, Physical of Ferromagnetism, second ed., Oxford University Press, 1997.
[25] A.L. Geiler, A. Yang, X. Zuo, S.D. Yoon, Y. Chen, V.G. Harris, C. Vittoria, Phys. Rev. Lett. 101 (2008) 067201.
[26] W. Zhang, Y. Bai, X. Han, L. Wang, X. Lu, L. Qiao, J. Alloys Comp. 546 (2013) 234.
[27] Y. Bai, J. Zhou, Z. Gui, L. Li, L. Qiao, J. Alloys Comp. 450 (2008) 412.
[28] J. Lee, Y.-K. Hong, W. Lee, G.S. Abo, J. Park, W.-M. Seong, W.-K. Ahn, J. Appl. Phys. 113 (2013) 073909.
[29] R. Sobiestianskas, B. Vengalis, J. Banys, J. Devenson, A.K. Oginskis, V. Lisauskas, L. Dapkus, Mater. Sci. – Poland 29 (2011) 41.
[30] M. Han, D. Liang, L. Deng, Appl. Phys. Lett. 90 (2007) 192507.
[31] M.L.S. Teo, L.B. Kong, Z.W. Li, G.Q. Lin, Y.B. Gan, J. Alloys Comp. 459 (2008) 567.